NASA TECHNICAL NOTE

NASA TN D-5225

NASA TN D-5225

c. 1

EXPERIMENTAL STUDY OF PUMP AND SEAL CHARACTERISTICS OF HELICAL GROOVE GEOMETRY INCORPORATED IN A COMBINED BEARING AND PUMP

by Lawrence P. Ludwig, Thomas N. Strom, and Robert L. Johnson

Lewis Research Center
Cleveland, Ohio

NATIONAL AERONAUTICS AND SPACE ADMINISTRATION • WASHINGTON, D. C. • MAY 1969

EXPERIMENTAL STUDY OF PUMP AND SEAL CHARACTERISTICS OF HELICAL GROOVE GEOMETRY INCORPORATED IN A COMBINED BEARING AND PUMP

By Lawrence P. Ludwig, Thomas N. Strom, and Robert L. Johnson

Lewis Research Center
Cleveland, Ohio

NATIONAL AERONAUTICS AND SPACE ADMINISTRATION

For sale by the Clearinghouse for Federal Scientific and Technical Information
Springfield, Virginia 22151 – CFSTI price $3.00

ABSTRACT

Combined bearing and pump rotors with 14.5° and 20° helix grooves were evaluated in a hermetically sealed pump. Oil, water, freon, and mercury were used in the studies at Reynolds numbers (based on clearance) between 2 and 2800. As predicted by theory, the pump pressure rise was linearly related to rotor peripheral velocity at low Reynolds numbers (2 to 12); however, between the investigated Reynolds numbers of 300 to 2800, the pump pressure rise varied with velocity raised to a power between 1.76 and 1.85. Above a Reynolds number of 1000, experimental friction factors were greater than that of other published experimental data. Maximum pump efficiencies were in the range of 2 to 3 percent for operation with water and freon. Torque data indicate that full fluid film lubrication was obtained with oil, water, freon, and mercury.

EXPERIMENTAL STUDY OF PUMP AND SEAL CHARACTERISTICS OF HELICAL GROOVE GEOMETRY INCORPORATED IN A COMBINED BEARING AND PUMP

by Lawrence P. Ludwig, Thomas N. Strom, and Robert L. Johnson

Lewis Research Center

SUMMARY

Pump pressure rise, flow rate, viscous losses, and sealing parameter were experimentally determined for a hermetically sealed pump consisting of a free-floating helical-groove rotor that served as a combined bearing and pump. Two rotors were evaluated: one had 14.5° helical grooves and the other had 20° helical grooves. Oil, water, freon, and mercury were used as the pumped fluids in studies where the Reynolds numbers (based on clearance) ranged from 2 to 2800.

The pump pressure rise was linearly related to rotor peripheral velocity in the low Reynolds number regime ($(Re)_c$ = 2 to 12) as predicted by the creeping flow theory. In the higher Reynolds number range investigated ($(Re)_c$ = 300 to 2800), the pump pressure rise was related to the velocity raised to a power between 1.76 and 1.85.

The friction factor data agree with other reported data in the Reynolds number range of 300 to 1000; above a Reynolds number of 1000, the magnitude of the friction factor was greater than other reported data. Maximum pump efficiencies were in the range of 2 to 3 percent for operation with water and freon, and the viscous losses for zero discharge were approximately 10 percent greater than that for maximum discharge flow.

The magnitude of the dimensionless sealing parameter λG is very close to that predicted by theory for the creeping flow regime; above a Reynolds number $(Re)_c$ of 400, reasonable agreement was obtained between experimentally determined sealing parameters and that predicted by turbulent viscoseal theory. Torque traces indicated that the combined pump and bearing operated with full fluid film lubrication in oil, water, freon, and mercury.

INTRODUCTION

The use of helical groove geometry has been investigated in studies of oil pumping that date back to 1922 (refs. 1 to 3). Most of the investigations since that time have been concerned with screw extruders for very viscous materials (refs. 4 to 10). Recent interest in the helical groove geometry has been in shaft seals without rubbing contact (viscoseals) for the space electric power generation systems such as SNAP-8 (ref. 11). High-speed rubbing contact leads to wear; therefore, pumps and seals without rubbing contact, such as the viscoseal, are potentially useful. In general, the viscoseal is attractive for sealing liquids that are highly corrosive or are poor lubricants, such as mercury for SNAP-8 or the high-temperature (1800° R or 1000 K) alkali metals employed in the Rankine cycle electric power generation system described in reference 12. Data on the sealing capability of viscoseals in alkali metals are given in references 11, 13, and 14, and sealing capability of the viscoseal operating in other media such as oil and water are given in reference 15.

In addition to sealing capability, pumping flow rate, pressure rise, and pumping efficiency are of interest since the helical groove geometry can function as a seal and as a pump to circulate the sealed fluid. Experimental data on the pumping efficiency of the viscoseal have not been found in the literature, and data on viscous losses or friction factor are limited.

Data generated in helical groove pumping tests could yield useful information for viscoseal design, and since the pump is fully flooded, gas ingestion is precluded. (It was shown in ref. 14 that gas ingestion, which probably affected much of the viscoseal data reported in the literature, can significantly influence experimental results.) Furthermore, in running the seal as a pump, only inlet and outlet pressures need be measured, thus circumventing measurement of pressures in a thin fluid film.

The helical groove geometry can function as a bearing as well as a seal or pump (ref. 16). Two of these functions can be combined to make a hermetically sealed pump in which the armature of an electric motor has helical grooves and serves as a combined bearing and pump. No shaft seals are needed. Such a device could be used to pump highly corrosive liquids, or liquids which are poor lubricants, since rubbing contact occurs only at startup or shutdown. However, since the pumping action originates principally from the viscous drag, the efficiency could be low.

The objectives of the present study were to

(1) Measure the pumping pressure rise and discharge flow of the helical groove geometry

(2) Measure the viscous losses and determine the efficiency of two helical groove geometries

(3) Determine the dimensionless sealing parameter of the pump running at zero discharge flow (sealing mode)

(4) Determine whether or not full fluid film lubrication is established when the helical groove geometry is used as a combined pump and bearing in a hermetically sealed pump

The pump consisted of a 2-inch- (5.08-cm-) diameter hermetically sealed free-floating rotor with helical grooves machined into the rotor outside diameter. The rotor was driven by a magnetic coupling. Oil, water, freon, and mercury were used as the pumped fluids at Reynolds numbers (based on clearance) from 2 to 2800. Rotors with grooves of 14.50° and 20° nominal helix angles were evaluated.

SYMBOLS

a'	land width, in.; cm
b'	groove width, in.; cm
C_1, C_2	functions of groove geometry, dimensionless
C_3, C_4	constants in eq. (2)
c	radial clearance, in.; cm
D	outside diameter of pump rotor, in.; cm
e	eccentricity, in.; cm
f	friction factor, dimensionless
G	geometry factor, dimensionless
h_0	groove depth, in.; cm
L	characteristic length, in.; cm
l	axial length of each pump section, in.; cm
$\dot{M}$	mass flow, lbm/sec; kg/sec
ΔP	pressure rise, lbf/in.^{2}; N/cm^2
Q	volume flow discharge, cu in./sec; cu cm/sec
Re^*	modified Reynolds number ($Re^* = (Re)_c(c/L)$)
$(Re)_c$	Reynolds number based on clearance ($(Re)_c = \rho Uc/\mu$)
r	radius of rotor, in.; cm
T	input torque, in.-lbf; cm-N

U	peripheral velocity of rotor, in./sec; cm/sec
α	groove helix angle, deg
β	ratio of groove depth plus radial clearance divided by radial clearance
λ	empirical sealing coefficient
λG	sealing parameter, dimensionless
μ	absolute viscosity, (lbf)(sec)/in.^{2}; (N)(sec)/cm^2
ρ	density, (lbf)(sec^2)/in.^{4}; (N)(sec^2)/cm^4

Superscript:

x	exponent or power of U

APPARATUS AND PROCEDURE

The hermetically sealed pump apparatus used in this study is shown schematically in figure 1(a). The apparatus consisted of a transparent acrylic plastic housing and a stainless-steel rotor that was coupled by permanent magnets to a variable-speed electric drive. The rotor speed was the same as the speed of the electric drive because both magnet coupling elements rotated in phase (no slippage). Two rotor geometries were evaluated: one had 14.5° helical grooves and the other had 20° grooves. Studies reported in reference 17 suggest that the 14.5° helix-angle selection is near the optimum; the 20° helix (fig. 1(b)) angle was selected for comparison. A groove depth h_0 3.1 times the radial clearance is reported in reference 17 to be near the optimum for viscoseals; for this study, groove-depth-to radial-clearance ratios of 2.6 and 3.2 were selected. Preliminary studies revealed that the pump flow discharge was enhanced and the viscous losses were minimized by selecting groove-width to land-width ratios greater than the theoretical optimum of 1.70 determined by creeping flow theory (ref. 17). Groove-width to land-width ratios selected were 4.46 and 3.59. The pertinent helical groove geometry is listed in table I. A spiral-groove pattern chemically etched on both end faces of the rotor (fig. 1) served as the thrust bearings. The thrust groove pattern was a 20° logarithmic spiral 0.002 inch (0.005 cm) deep. The variable-speed electric drive motor permitted operation between 0 and 3000 rpm, and input torque was measured by a rotating slip-ring torque meter. Pressure rise across the pump (viscoseal) was measured by a differential-type strain-gage transducer; one side of the pressure transducer was connected to the pump inlet and the other side to the outlet. The temperature was measured at the inlet and at the discharge end of the helical pump by thermocouples submerged in the fluid. Fluid flow was from the reservoir to the inlet feed holes at the

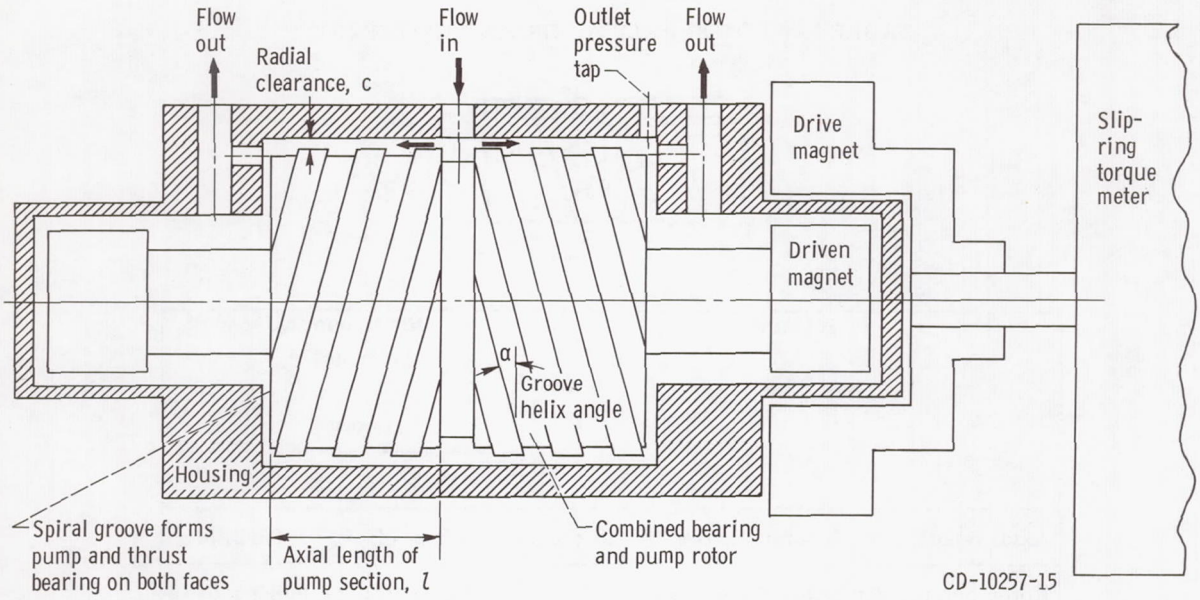

(a) Hermetically sealed pump.

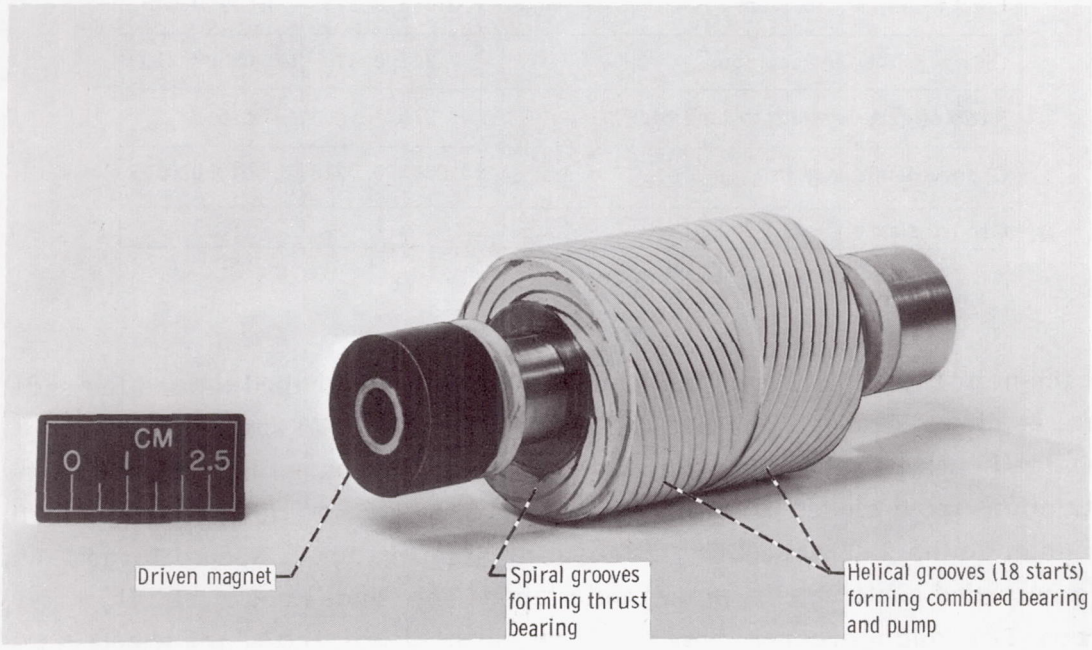

C-68-3333

(b) Combined bearing and pump rotor, 20° helix-angle grooves.

Figure 1. - Hermetically sealed pump apparatus and rotors.

TABLE I. - ROTOR HELICAL GROOVE GEOMETRY

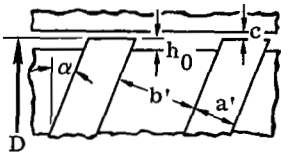

Geometry	Rotor nominal helix angle, α, deg	
	14.5	20
Axial length of each pump section, ℓ, in.; cm	1.08; 2.74	1.08; 2.74
Rotor outside diameter, D, in.; cm	1.9988; 5.0769	1.9985; 5.0762
Radial clearance, c, in.; cm	0.0026; 0.0066	0.0027; 0.0069
Land width, a', in.; cm	0.068; 0.173	0.019; 0.048
Groove width, b', in.; cm	0.244; 0.620	0.086; 0.218
Ratio of groove width to land width, b'/a'	3.6	4.5
Groove depth, h_0, in.; cm	0.0085; 0.0216	0.0070; 0.0178
Groove starts	5	18

center of the helical pump. From the center, the fluid was pumped toward the ends by two helical sections, each 1.08 inches (2.74 cm) in length ℓ. From the ends, the flow was discharged back into the reservoir. A valve in the discharge line permitted various flow restrictions from closed to full-open discharge. Flow was measured by a turbine-type flowmeter in the discharge line. Pressures, temperatures, speed, torque, and flow were recorded continuously on magnetic tape. The fluids used were oil, water, freon (freon-TF), and mercury; their pertinent physical properties are listed in table II. In any one run, the fluid temperature change was limited to 6° F (3.3 K) to minimize dimensional changes that affect the radial clearance between the housing and the rotor.

TABLE II. - DATA USED TO INTERPOLATE VALUE OF FLUID PHYSICAL PROPERTIES AT OPERATING TEMPERATURES

Fluid	Temperature		Density, ρ		Absolute viscosity, μ	
	^{o}F	K	$(lbf)(sec^2)/in.^4$	$(N)(sec^2)/cm^4$	$(lbf)(sec)/in.^2$	$(N)(sec)/cm^2$
Oil Mil-H-5606B	70	294	7.72×10^{-5}	8.23×10^{-6}	2.76×10^{-6}	1.90×10^{-6}
	80	300	7.68	8.18	2.25	1.55
	90	305	7.65	8.15	1.96	1.35
Water	70	294	9.34×10^{-5}	9.96×10^{-6}	13.89×10^{-8}	9.58×10^{-8}
	80	300	9.32	9.94	12.50	8.62
	90	305	9.31	9.92	11.11	7.66
Freon (freon-TF)	70	294	1.47×10^{-4}	1.57×10^{-5}	10.42×10^{-8}	7.18×10^{-8}
	80	300	1.46	1.55	9.72	6.70
	90	305	1.45	1.54	9.03	6.22
Mercury	70	294	1.27×10^{-3}	1.35×10^{-4}	2.22×10^{-7}	1.53×10^{-7}
	80	300	1.27	1.35	2.15	1.48

RESULTS AND DISCUSSION

Helical Groove Pump Theory

Insight into the relation between outlet pressure and mass flow of the helical groove pump can be gained from an equation that is valid only in the creeping flow regime. This equation, given in reference 18 is

$$Q = \underbrace{C_1 \frac{\pi D U c}{2}}_{\substack{\text{drag} \\ \text{flow}}} - \underbrace{C_2 \frac{\pi D c^3 \Delta P}{12 \mu l}}_{\substack{\text{pressure} \\ \text{flow}}} \tag{1}$$

in which

Q volume flow, cu in./sec; cu cm/sec

C_1 function of groove geometry

D outside diameter of pump rotor, in.; cm

U peripheral velocity of rotor, in./sec; cm/sec

c radial clearance, in.; cm

C_2 function of groove geometry

ΔP pressure rise, lbf/in.^{2}; N/cm^2

μ absolute viscosity, (lbf)(sec)/in.^{2}; (N)(sec)/cm^2

l pump axial length, in.; cm

Equation (1) reduces to the following linear relation for a given fluid, temperature, pump diameter, and clearance:

$$Q = C_3 U - C_4 \frac{\Delta P}{l} \tag{2}$$

The preceding equation predicts the outlet pressure and volume flow relation illustrated in figure 2, where the axial pressure gradient $\Delta P/l$ is plotted as a function of the volume flow discharge Q. The maximum pressure gradient occurs at zero flow (Q = 0) and has an ordinate intercept value of C_3U/C_4. The maximum flow Q occurs at zero pressure gradient and has an abscissa intercept value of C_3U. For a given speed, the pressure and flow relation is defined by a straight line between these two intercepts. If the pumped speed is doubled, a new line can be constructed parallel to the original line, but it will have intercept values twice the original intercept values. Thus, for equal-increment changes in speed, a family of equally spaced, parallel, straight lines can be constructed to form a theoretical performance map for the creeping flow regime.

In general, the seal and pump flow regimes of engineering interest in space power systems are above the creeping flow regime, and fluid turbulence and inertial effects should be expected. The importance of fluid inertia effects in helical groove pumping devices was first pointed out in reference 16 where it is postulated that inertia effects become significant at modified Reynolds numbers greater than 1. Thus, above a modified Reynolds number of 1, the predictions from equation (1) should deviate from experimental results. The modified Reynolds number developed in reference 16 for the fluid film in the helical geometry is

$$Re^* = (Re)_c \frac{c}{L} = \frac{\rho U c^2}{\mu L} \tag{3}$$

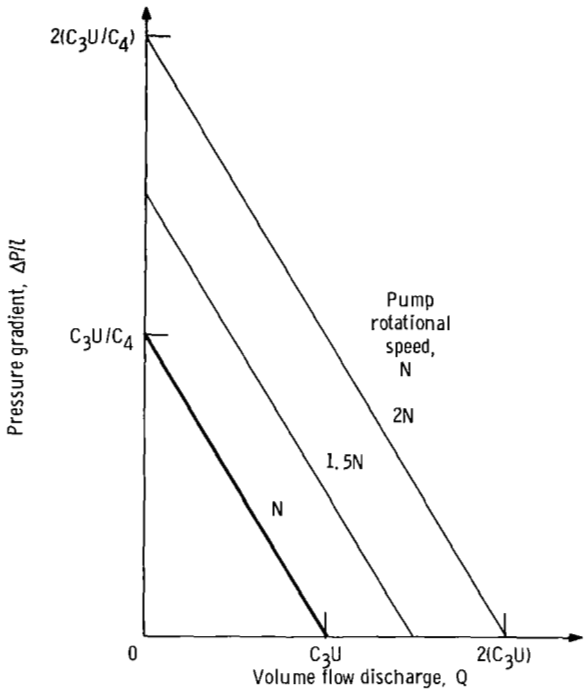

Figure 2. - Pressure rise and discharge flow relation for helical groove geometry operating in isothermal creeping flow regime.

where

Re*	modified Reynolds number
$(Re)_c$	fluid film Reynolds number based on clearance
c	radial clearance, in.; cm
L	characteristic length, circumferential length of one groove-land pair, in.; cm
ρ	density, $(lbf)(sec^2)/in.^4$; $(N)(sec^2)/cm^4$
U	peripheral velocity of rotor, in./sec; cm/sec
μ	absolute viscosity, $(lbf)(sec)/in.^2$; $(N)(sec)/cm^2$

Experimentally Determined Pressure Rise and Discharge Flow

The pressure rise as a function of the discharge mass flow of oil is shown in figure 3 for the hermetically sealed pump depicted schematically in figure 1. The data presented are for a flow regime between a Reynolds number $(Re)_c$ (based on clearance) of 2.5 and 12. At a given discharge flow, the pressure rise is, for practical purposes,

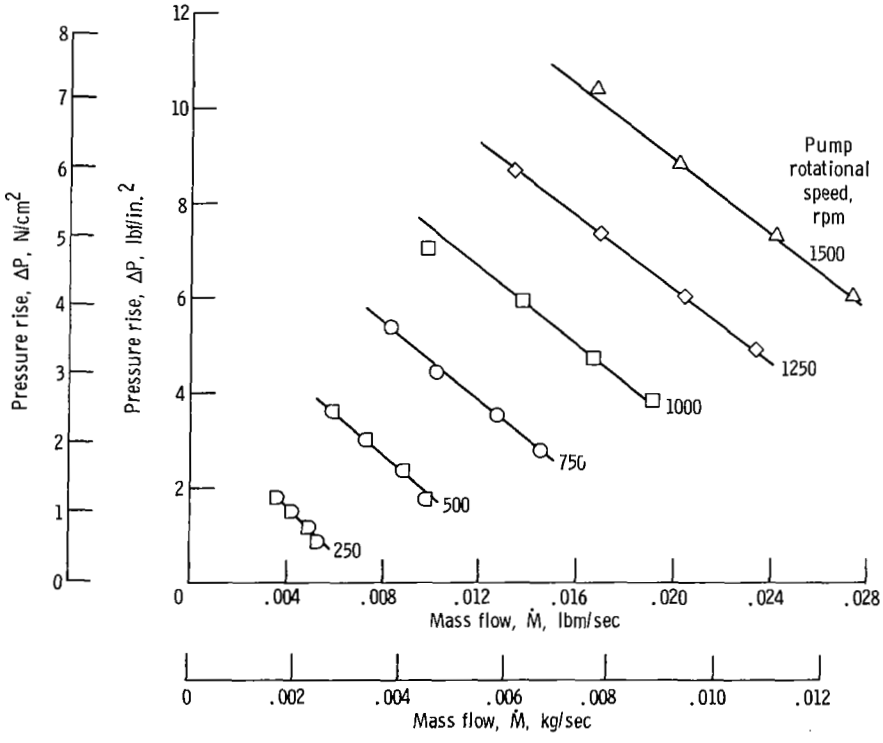

Figure 3. - Pressure rise as function of pump discharge mass flow for various rotational speeds. Fluid, oil; groove helix angle, 14.5°; fluid temperature, 80° F (299.8 K); Reynolds number (based on clearance), 2.5 to 12; modified Reynolds number, 0.005 to 0.024.

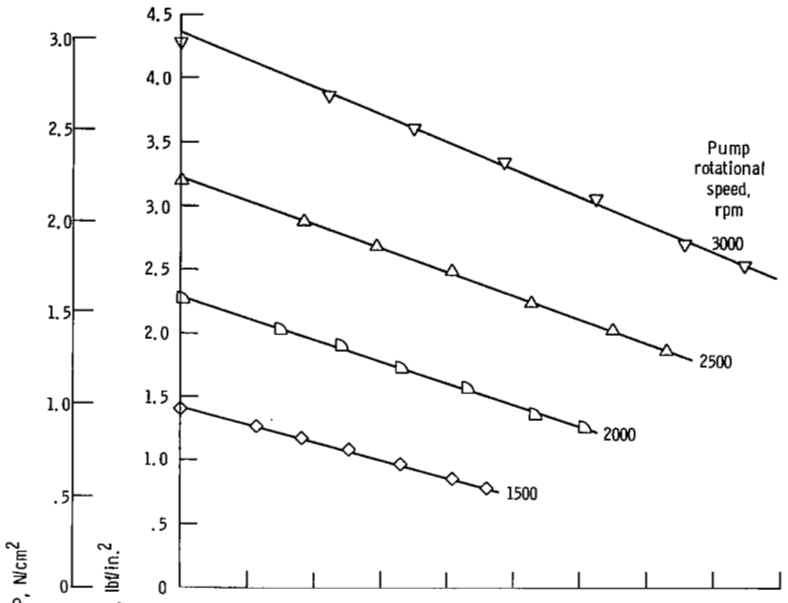

(a) Fluid water; groove helix angle, 14.5°; fluid temperature, 77.8° to 79.7° F (298.6 to 299.6 K); Reynolds number (based on clearance), 303 to 613; modified Reynolds number, 0.6 to 1.2.

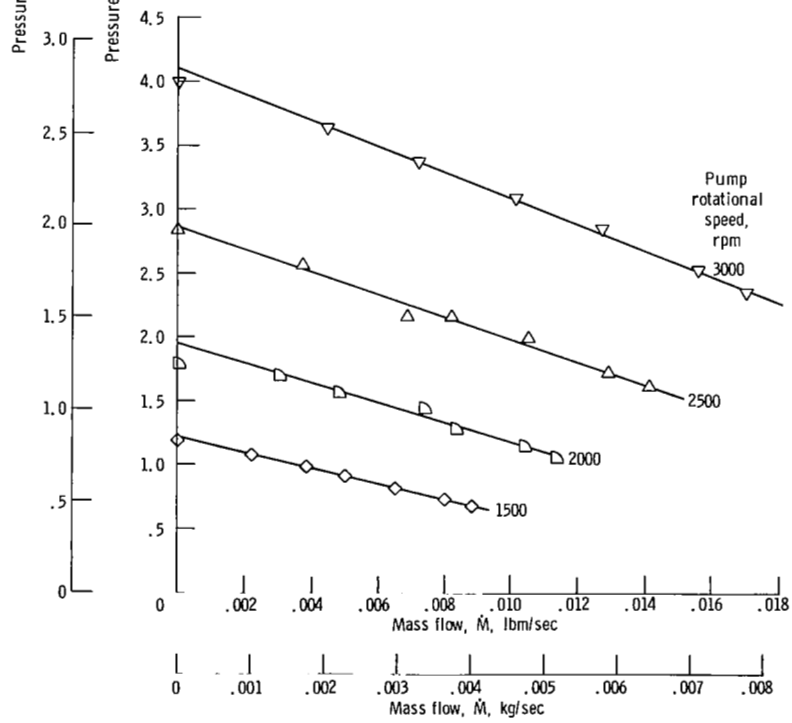

(b) Fluid, water; groove helix angle, 20°; fluid temperature, 79.5° to 80.5° F (299.5 to 300.1 K). Reynolds number (based on clearance), 324 to 657; modified Reynolds number, 2.5 to 5.1.

Figure 4. - Pressure rise as function of pump discharge mass flow for various pump rotational speeds.

a linear function of the pump speed predicted by the creeping flow theory. However, in other experiments at higher Reynolds numbers, nonlinear effects are evident in the performance maps of pressure rise as a function of mass flow of water and freon at various pump rotational speeds from 1500 to 3000 rpm (fig. 4). The data show a linear relation between mass flow and pressure rise for each pump speed, and this linear relation holds for both pump geometries (20° and 14.5° helix angle) and both fluids (water and freon). However, for equal increments of speed increase (1500 to 2000 to 2500 rpm, etc.), the pressure rise increments are not equal, as predicted by the creeping flow analysis. These data suggest that for the flow regime above creeping flow the form of equation (2) could be expressed emiprically as

$$Q = C_3 U^x - C_4 \frac{\Delta P}{l} \tag{4}$$

where x is a power greater than 1.

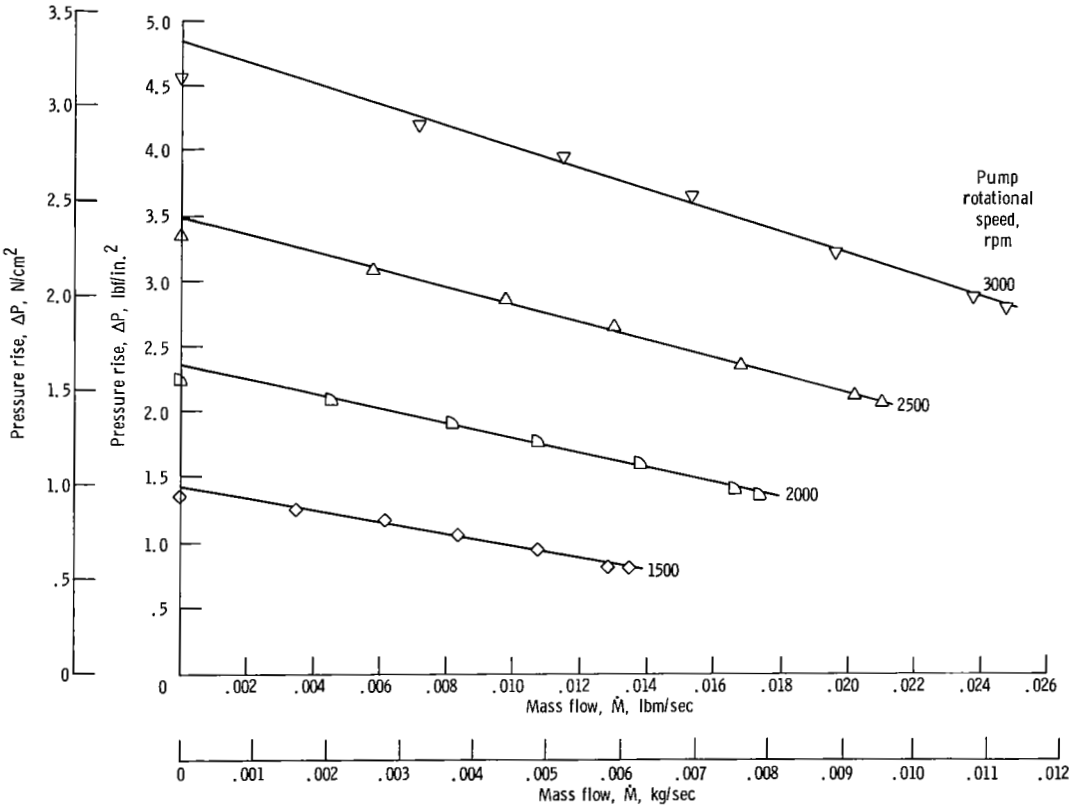

(c) Fluid, Freon-TF; groove helix angle, 14.5°; fluid temperature, 81.3° to 83.6° F (300.5 to 301.8 K); Reynolds number based on clearance, 615 to 1240; modified Reynolds number, 1.3 to 2.6.

Figure 4. - Continued.

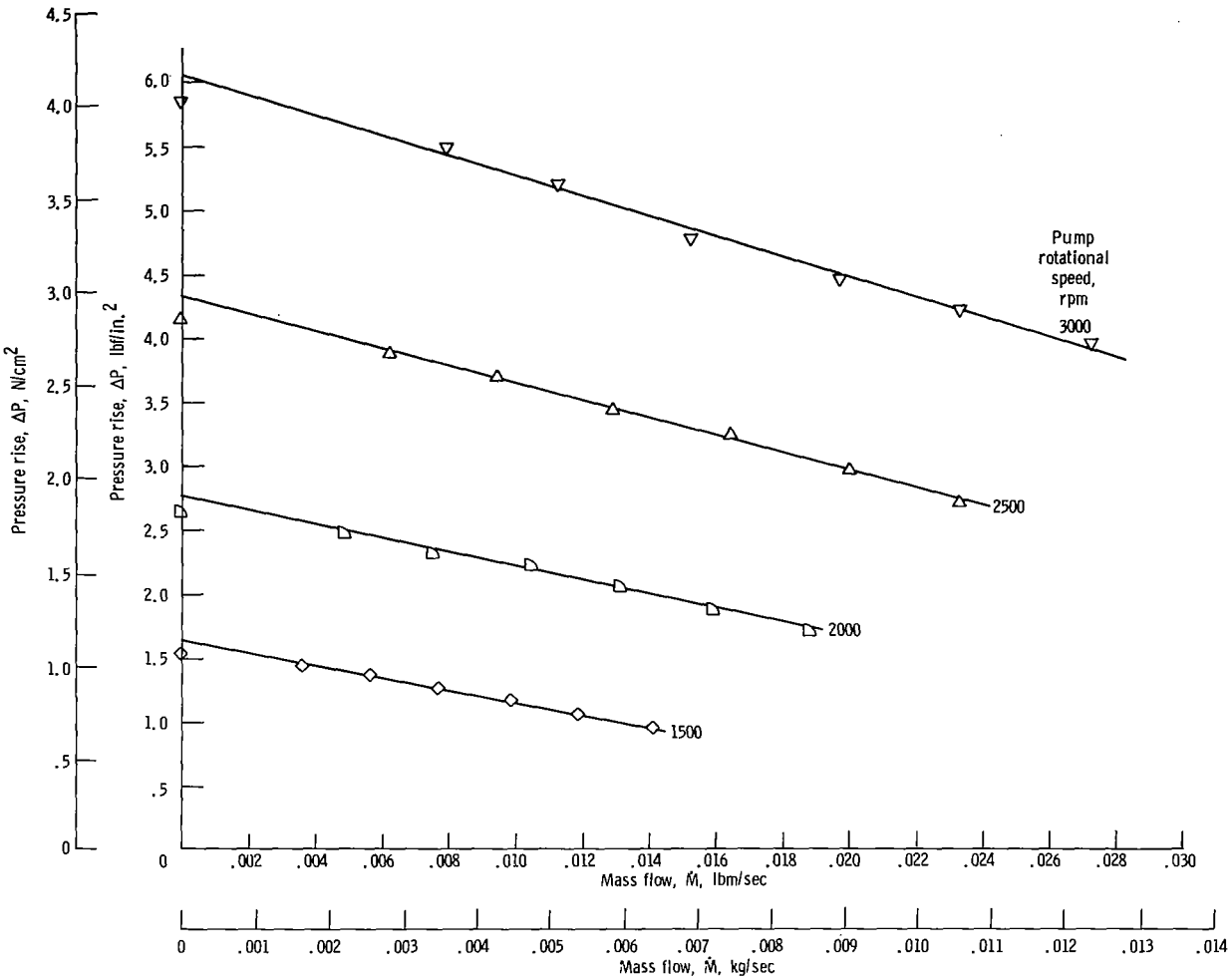

(d) Fluid, Freon-TF; groove helix angle, 20°; fluid temperature 76.1° to 80.9° F (297.6 to 300.3 K); Reynolds number based on clearance, 637 to 1290; modified Reynolds number, 5.0 to 10.2.

Figure 4. - Concluded.

Effect of Rotor Peripheral Velocity

The effect of velocity on pressure rise (or value of power x) can be evaluated by considering the pressure gradient $\Delta P/l$ produced at zero discharge (sealing mode). For zero discharge, equation (4) becomes

$$\frac{\frac{\Delta P}{l}}{U^x} = \frac{C_3}{C_4} = \text{Constant} \tag{5}$$

TABLE III. - RELATION OF PRESSURE GRADIENT TO ROTOR PERIPHERAL VELOCITY FOR ZERO NET FLOW DISCHARGE (SEALING MODE)

Run	Fluid	Rotor helix angle, α, deg	Fluid temperature,		Rotor speed, rpm	Rotor peripheral velocity, U		Reynolds number (based on clearance), $(Re)_c$	Pressure gradient, $\Delta P/l$		Power of U used to reduce pressure gradient factor, to mean constant value	Actual value of pressure gradient factor, $(\Delta P/l)/U^x$	Mean constant value of pressure gradient factor, $(\Delta P/l)/U^x$	Derivation from mean, percent
			^oF	K		in./sec	cm/sec		lbf/cu in.	N/cu cm				
1	Water	14.5	79.7	299.7	1500	157.1	399.0	303	1.30	0.35	1.76	0.000181	0.000170	6
			79.8	299.7	2000	209.4	531.9	405	2.10	.57		.000174		2
			80.0	299.8	2500	261.8	664.0	506	2.96	.80		.000165		3
			80.5	300.1	3000	314.2	798.1	613	3.96	1.07		.000160		6
2	Water	20.0	80.6	300.2	1500	157.1	399.0	324	1.09	3.0	1.76	0.000148	0.000148	0
			81.1	300.4	2500	261.8	664.0	544	2.62	.71		.000146		1
			81.4	300.6	3000	314.2	798.1	657	3.70	1.00		.000150		1
3	Freon	14.5	83.6	301.8	1500	157.1	399.0	615	1.25	0.34	1.78	0.000154	0.000154	0
			83.8	301.9	2000	209.4	531.9	820	2.08	.56		.000155		<1
			84.2	302.1	2500	261.8	664.0	1028	3.10	.84		.000154		0
			84.9	302.5	3000	314.2	798.1	1240	4.23	1.15		.000153		<1
4	Freon	20.0	80.7	300.2	1500	157.1	399.0	637	1.41	0.38	1.85	0.000122	0.000127	4
			81.0	300.4	2000	209.4	531.9	851	2.46	.67		.000126		1
			81.5	300.6	2500	261.8	664.0	1068	3.84	1.04		.000129		2
			82.6	301.2	3000	314.2	798.1	1290	5.42	1.47		.000131		3
5	Mercury	20.0	86.0	303.2	800	84.0	213.4	1333	2.92	0.79	1.84	0.000841	0.000856	2
					1000	104.4	265.2	1666	4.49	1.22		.000867		1
					1200	124.8	317.0	2000	6.20	1.68		.000862		1
					1400	146.4	371.8	2335	8.15	2.21		.000844		1
					1600	166.8	423.7	2672	10.65	2.89		.000868		1

From the pressure gradient and velocity data, the power x necessary to satisfy the above equation can be evaluated. Table III gives the results of this evaluation for water, freon, and mercury. In the flow regime of Reynolds numbers (based on clearance) from 300 to 2800, a near constant value for C_3/C_4 is found for each fluid and rotor combination by raising the velocity U to a power between 1.76 and 1.85. In general, the larger exponential powers are associated with the larger Reynolds numbers, which suggests that the exponent may increase with increasing Reynolds number and thus approach the velocity-squared relation suggested in reference 16. The data presented in table III are not intended to establish a value for the exponent; rather, their purpose is to point out the nonlinear effect of velocity on the pressure

Viscous Losses and Efficiency

Friction factor. - The friction factor at pump zero net discharge (sealing mode) as a function of Reynolds number (based on clearance) is shown in figure 5 for water, freon, and mercury. The friction factor was calculated from the formula for journal bearings (ref. 19)

$$f = \frac{T}{\pi \rho U^2 r^2 l} \tag{6}$$

where

T input torque, in.-lbf; cm-N

U peripheral velocity of rotor, in./sec; cm/sec

r rotor radius in.; cm

l pump axial length, in.; cm

Experimental viscoseal friction factor data from other references are plotted in figure 5(a). The data are not exactly comparable because of geometric differences at the ends of the rotor (thrust bearings and magnets). However, measurements indicate that the torque which can be attributed to the thrust bearing and magnets (end effects) is between 5 to 10 percent of the total torque measured. In the region of Reynolds number from 300 to 1000, the experimental data fall within the experimental scatter band width given by reference 15. The significant deviation from reported experimental data (refs. 13 and 15) is in the Reynolds number above 1000. This deviation could be attributed to gas

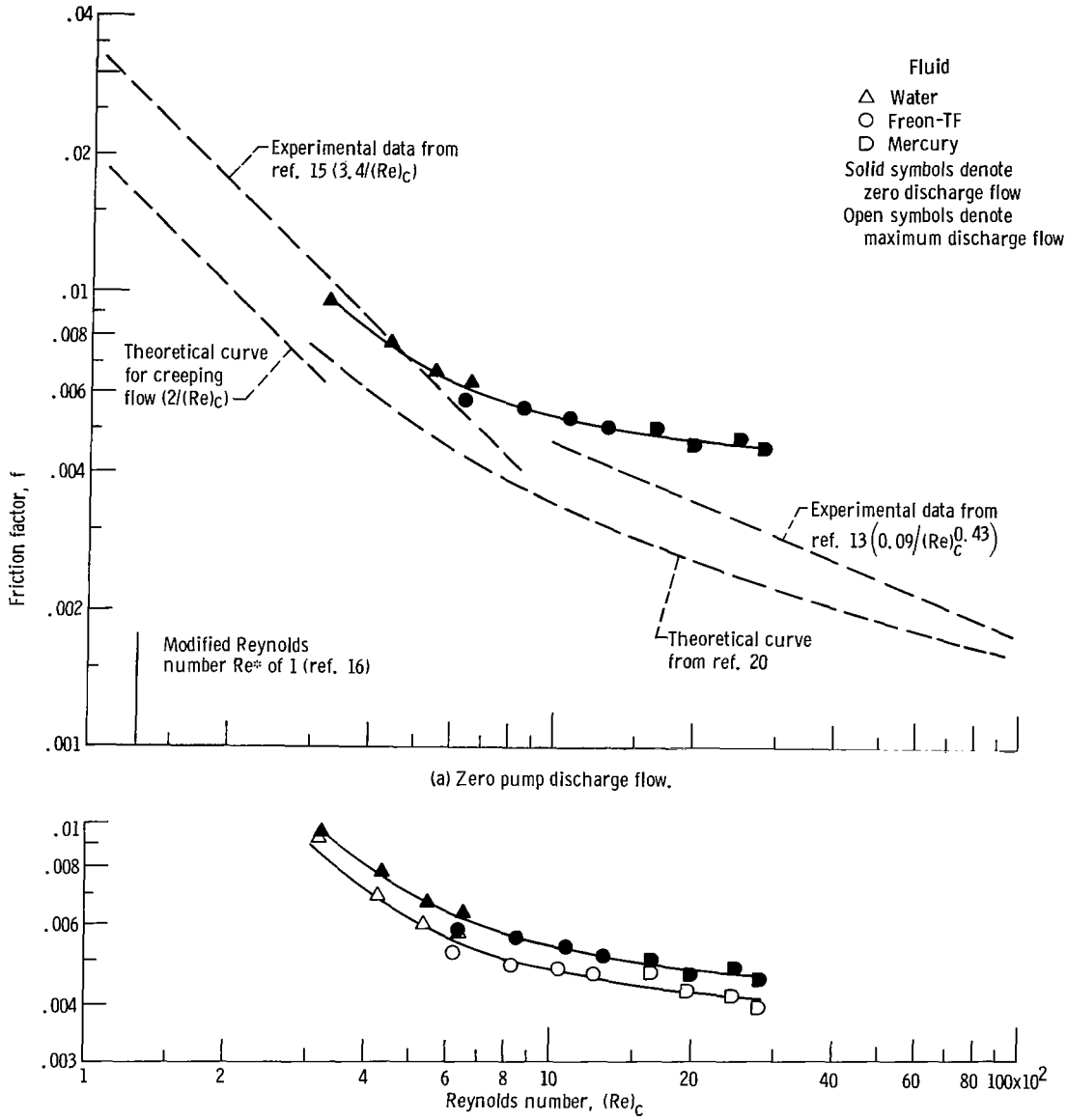

(a) Zero pump discharge flow.

(b) Zero and maximum pump discharge flows.

Figure 5. - Friction factor as function of Reynolds number. Rotor helix angle, 20°.

ingestion. Much of the viscoseal data reported in the literature is affected by gas ingestion which tends to reduce the friction factor because of the presence of the gas in the sealed liquid; in this study the fully flooded rotor operated without gas ingestion. Theoretical journal bearing friction factors for creeping flow and for turbulent flow (ref. 20) are included for comparison purposes.

The friction factors for zero discharge (sealing mode) and for maximum pump discharge are presented in figure 5(b). The friction factors for intermediate pump discharge flows fall between the two curves indicated. The results indicate that the magnitude of the pump flow affects the frictional loss, but the effect is small (approximately 10 percent difference between zero and maximum discharge).

Pumping efficiency. - Figure 6 shows pump efficiency as a function of pump hydraulic power output. Pump efficiency was calculated from

$$\% \text{ Efficiency} = \frac{\text{Hydraulic power output}}{\text{Power input}} \times 100 \tag{7}$$

The pump hydraulic power output is defined as the product of the outlet pressure and the volume flow; the power input was calculated from the input torque and speed. In general, the efficiency is low (1- to 3-percent range) for both pump geometries (20° and 14.5° helix angle) and for both water and freon. The maximum efficiency is at maximum flow, which occurs when the pump outlet pressure is minimum (full-open discharge). For example, inspection of figure 6(a) reveals that for a pump speed of 2000 rpm, the maximum efficiency occurs at full-open discharge; as the pump outlet restriction is increased, the power out decreases, hence, the pump efficiency decreases. The peak output power reached at full-open discharge for each speed forms a locus of points that defines the maximum pump flow capability for the discharge line resistance inherent in the apparatus. This locus of points suggests a maximum efficiency in the range of 2 to 3 percent for both pump geometries when pumping water and freon.

Comparison of figures 6(a) and (b), for a 14.5° and a 20° helix-angle pump, respectively, reveals that when it is pumping water, the 14.5° helix-angle pump has the highest efficiency. The opposite is true when it is pumping freon (fig. 6(c)), which suggests that each fluid type may have a different optimum pump geometry. No attempt was made in this study to maximize the efficiency through alteration of the rotor geometries.

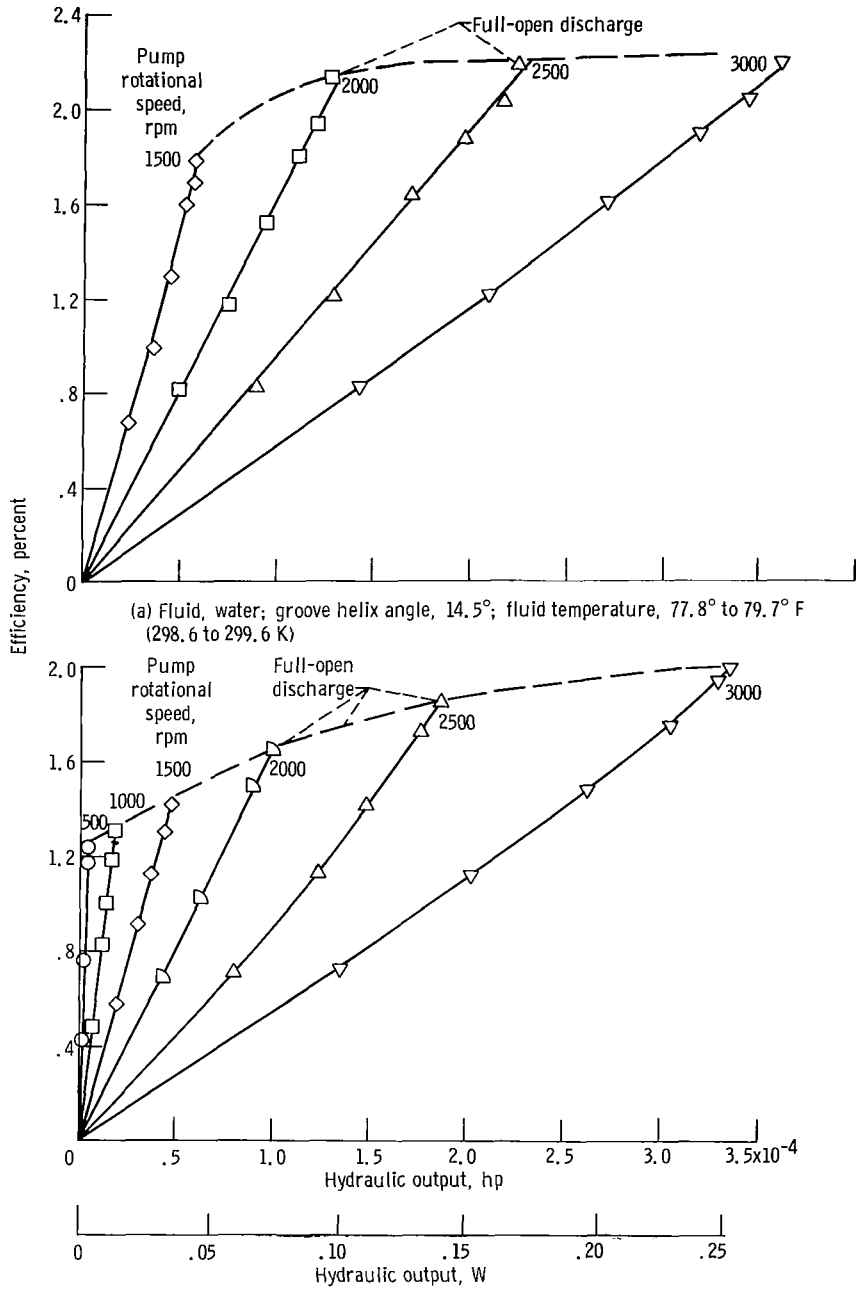

(b) Fluid, water; groove helix angle, 20°; fluid temperature, 79.5° to 80.5° F (299.5 to 300.1 K).

Figure 6. - Pumping efficiency as function of power output.

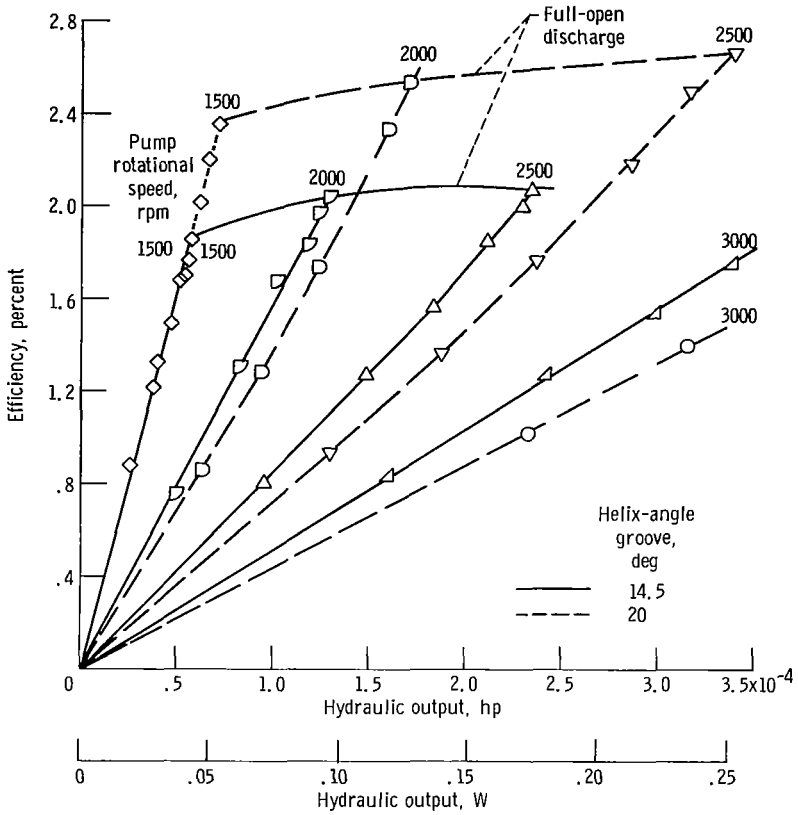

(c) Fluid, Freon-TF; groove helix angles, 14.5° and 20°; fluid temperature, 76.1° to 83.6° F (297.6 to 301.8 K).

Figure 6. - Concluded.

Sealing Parameter

When the helical groove geometry is used in a sealing mode (no discharge flow), the expression for the sealing capacity for slow creeping flow regime can be obtained from equation (1) by setting Q = 0. Therefore,

$$G = \frac{c^2 \Delta P}{6U\mu l} \tag{8}$$

where

G geometry factor, dimensionless function of helix geometry equal to C_1/C_2 (see eq. (1))

ΔP pressure rise lbf/in.^{2}; N/cm^2

Equation (8) was modified in reference 14 to include an empirical sealing coefficient λ to take into account the effects of fluid inertia, eccentricity, machining variations, turbulence, and gas ingestion. The dimensionless sealing parameter λG is taken as a measure of the sealing capacity and embodies the geometry factor G and the empirical sealing coefficient λ. An increase in the sealing parameter λG indicates an increase in the sealing capability.

A plot of the sealing parameter obtained with the pump running under zero discharge conditions is shown in figure 7. The advantages of obtaining viscoseal sealing parameters by running the helical grooves fully flooded with zero net output flow (shutoff pump) are that

(1) No question arises as to the seal wetted length since the entire rotor is flooded. Thus, pressures do not have to be measured in the thin fluid film to establish the pressure gradient.

(2) Operation in the fully flooded mode eliminates the problem of gas ingestion.

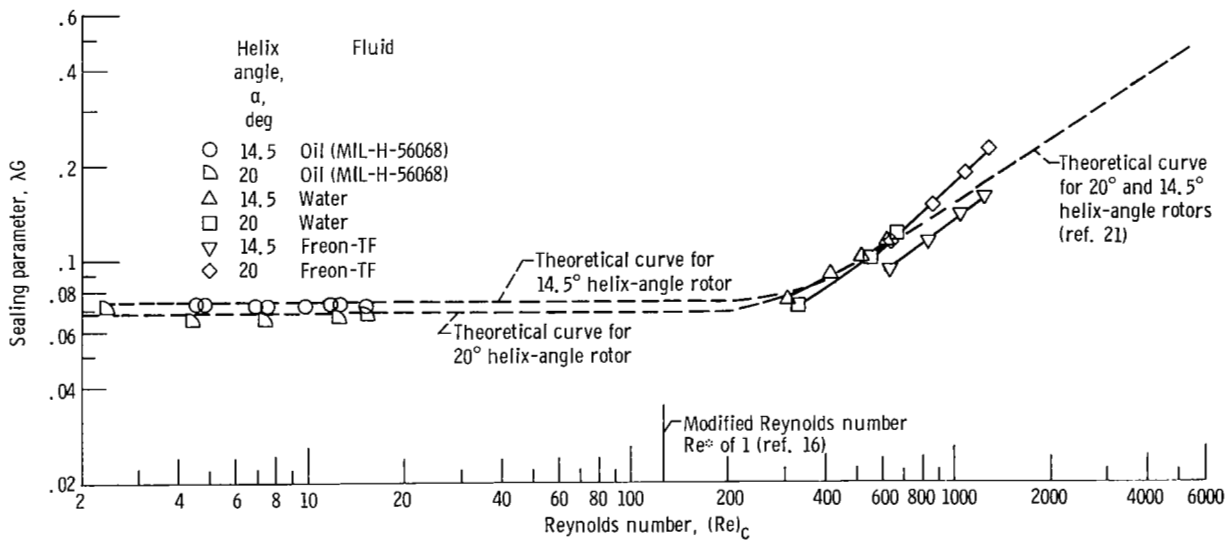

Figure 7. - Sealing parameter as function of Reynolds number (based on clearance).

Inspection of curves in figure 7 reveals that, in general, the 14.5° helix-angle rotor produces a higher sealing parameter than that of the 20° helix-angle rotor when it is sealing water, particularly in the lower Reynolds number range. However, extrapolation of these two curves suggests that the 20° helix-angle rotor may be better above a Reynolds number of 700. When it is sealing freon, the 20° helix-angle rotor produces a sealing parameter near that of the 14.5° helix-angle rotor.

Above a Reynolds number of 400, the data show reasonable agreement with the theory for the turbulent regime (ref. 21). However, the data trend indicates that the transition to the laminar region at a Reynolds number below 400 may not level off at the constant value of approximately 0.07 as predicted by the theory. For operation with oil at Reynolds numbers between 2 and 12, the experimental data for both the 14.5° and 20° helix-angle rotors was very close to that predicted by theory (ref. 18).

The rotor probably operated with eccentricities ranging from a condition in which the rotor was touching the housing (e = c) to a condition of nearly full concentricity (e = 0). With respect to this operation, other viscoseal observations at the Lewis Research Center suggest that eccentricity has a negligible effect on the overall sealing parameter.

Full Film Lubrication

Torque as a function of rotor speed is shown in figure 8 for the pump of figure 1 operating with water at a constant pump outlet restriction that permitted approximately one-half the maximum discharge flow at each speed. All torque traces were very similar in shape from zero pump discharge to maximum discharge; the torque magnitude variation with discharge rate is reflected in the friction factors plotted in figure 5(b). Just as in the friction curve for journal bearings (ref. 22), the shape of the torque trace indicates the speed at which lift-off occurs.

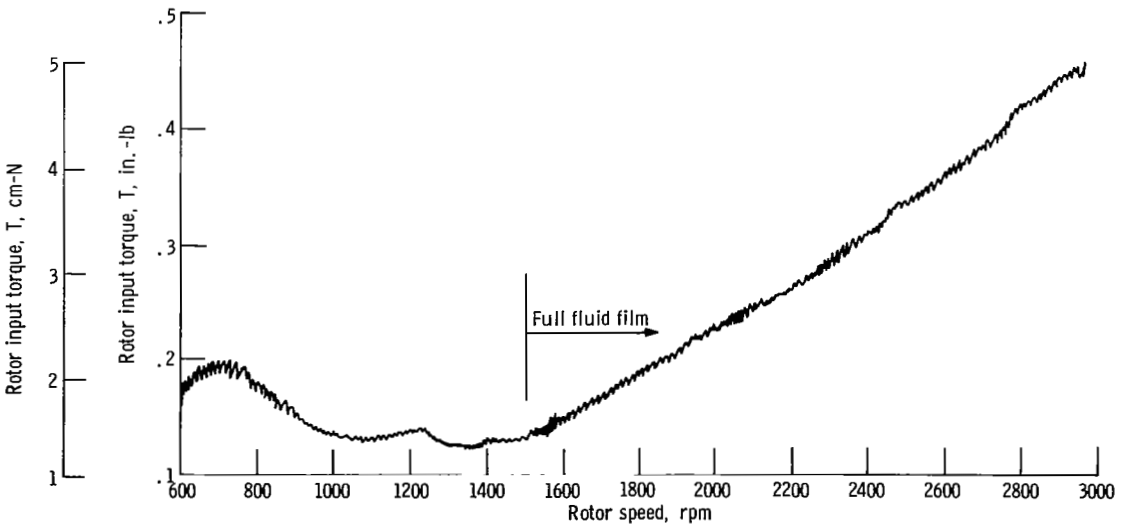

Figure 8. - Rotor input torque as function of rotor speed. Fluid, water; groove helix angle, 20°; flow, one-half maximum discharge at each speed (constant outlet restriction).

At low speeds of 600 to 1500 rpm, the torque trace suggests rotor-to-housing contact, or boundary lubrication; near 1500 rpm, the slope of the curve indicates a torque and speed relation characteristic of full fluid film lubrication. For operation in oil, the lift-off speed (point of initiation of full fluid film lubrication) occurred at speeds lower than 200 rpm. Table IV gives the fluid, operating temperature, and lift-off speed observed for oil, water, freon, and mercury.

TABLE IV. - ROTOR SPEEDS REQUIRED TO ESTABLISH FULL FLUID FILM LUBRICATION (LIFT-OFF SPEEDS)

Fluid	Rotor helix angle, α, deg	Fluid temperature		Lift-off speed, rpm
		^{o}F	K	
Oil	14.5	76	297.6	<200
	20.0	80	299.8	<200
Water	14.5	~74	296.5	1600
	20.0	~76	297.6	1500
Freon-TF	14.5	~77	298.1	1500
	20.0	~75	297.0	1500
Mercury	14.5	~84	302.0	750
	20.0	~84	302.0	<700

SUMMARY OF RESULTS

A hermetically sealed pump consisted of a free-floating rotor with helical grooves on the outside diameter was constructed. The rotor, acting as a combined bearing and pump, was driven by a magnetic coupling. The pump discharge flow rate, pressure rise, and viscous losses were measured using oil, water, freon, and mercury as the pumped fluids. Two rotors, one with 14.5^{o} and the other with 20^{o} grooves, were used in the studies covering a range of Reynolds number (based on radial clearance) from 2 to 2800. The following pertinent results were obtained for the pumping pressure rise and discharge flow for two investigated flow regimes:

1. In the flow regime of Reynolds numbers between 2 and 12, the output pressure was linearly related to rotor peripheral velocity at a given mass flow, as predicted by creeping flow analysis; the relation between pump outlet pressure and mass discharge flow was linear.

2. In the flow regime of Reynolds numbers between 300 and 1200 (water and freon studies), the output pressure was not linearly related to rotor peripheral velocity. The data at zero discharge indicated that the pressure was related to the rotor peripheral velocity raised to a power between 1.76 and 1.85; the relation between pump outlet pressure and mass discharge flow was linear.

The following results were obtained for the viscous losses and pumping efficiency:

3. The experimental friction factor data agree with other reported data in the flow regime between a Reynolds number (based on clearance) of 300 and 1000. Above a Reynolds number of 1000, the data indicated friction factors greater than other reported data.

4. The friction factor for zero mass flow (sealing mode) was approximately 10 percent greater than that for maximum pump discharge.

5. For water and freon, extrapolations indicated a pump efficiency in the range of 2 to 3 percent for both the 20° and 14.5° helix-angle pump. The highest efficiency was reached at maximum pump discharge.

The following results were obtained with respect to the dimensionless sealing parameter:

6. The dimensionless sealing parameter λG agreed with that predicted by creeping flow theory in a flow regime for the range of Reynolds number 2 to 12. This agreement was attained for both the 14.5° and 20° helix-angle geometries operating in oil. Reasonable agreement was obtained with turbulent flow theory for viscoseals in the flow regime for the range of Reynolds number 400 to 1300 for water and freon.

7. With respect to the onset of full fluid film lubrication, results showed that the helical grooved rotor can function as a combined free-floating bearing and pump. Torque traces indicated that full film lubrication was established for oil, water, freon, and mercury.

Lewis Research Center,
National Aeronautics and Space Administration,
Cleveland, Ohio, December 27, 1968,
120-27-04-90-22.

REFERENCES

1. Rowell, H. S.; and Finlayson, D.: Screw Viscosity Pumps. Engineering, vol. 114, Nov. 17, 1922, pp. 606-607.

2. Rowell, H. S.; and Finlayson, D.: Screw Viscosity Pumps. Engineering, vol. 126, Aug. 31, 1928, pp. 249-250.

3. Rowell, H. S.; and Finlayson, D.: Screw Viscosity Pumps. Engineering, vol. 126, Sept. 28, 1928, pp. 385-387.

4. Rogowsky, Z.: Mechanical Principles of the Screw Extrusion Machine. Engineering, vol. 162, no. 4213, Oct. 11, 1946, pp. 358-360.

5. Strub, R. A.: Spindle Drag Pump. Machine Des., vol. 25, July 1953, pp. 149-151.

6. Pigott, W. T.: Pressures Developed by Viscous Materials in the Screw Extrusion Machine. Trans. ASME, vol. 73, no. 7, Oct. 1951, pp. 947-955.

7. Members of the Polychemicals Department, E.I. du Pont de Nemours and Co.: Theory of Extrusion. Ind. Eng. Chem., vol. 45, no. 5, May 1953, pp. 969-993.

8. Eccher, Silvio; and Valentinotti, Aldo: Experimental Determination of Velocity Profiles in an Extruder Screw. Ind. Eng. Chem., vol. 50, no. 5, May 1958, pp. 829-836.

9. Griffith, R. M.: Fully Developed Flow in Screw Extruders. Ind. Eng. Chem. Fundamentals, vol. 1, no. 3, Aug. 1962, pp. 180-187.

10. Squires, P. H.: Screw Extrusion - Flow Patterns and Recent Theoretical Developments. SPE Trans., vol. 4, no. 1, Jan. 1964, pp. 7-16.

11. Lessley, R. L.: SNAP-8 Seals-To-Space Development Test Program. Volume I: Visco Pump. Rep. 280 8, vol. 1, Aerojet-General Corp. (NASA CR-54234, vol. 1), May 1964.

12. Bisson, Edmond E.; and Anderson, William J.: Advanced Bearing Technology. NASA SP-38, 1964, p. 461.

13. King, Alan E.: Screw Type Shaft Seals for Potassium Lubricated Generators. IEEE Trans. on Aerospace, vol. AS-3, Suppl., June 1965, pp. 471-479.

14. Ludwig, Lawrence P.; Strom, Thomas N.; and Allen, Gordon P.: Gas Ingestion and Sealing Capacity of Helical Groove Fluid Film Seal (Viscoseal) Using Sodium and Water as Sealed Fluids. NASA TN D-3348, 1966.

15. McGrew, J. M.; and McHugh, J. D.: Analysis and Test of the Screw Seal in Laminar and Turbulent Operation. J. Basic Eng., vol. 87, no. 1, Mar. 1965, pp. 153-162.

16. Zuk, John; Ludwig, Lawrence P.; and Johnson, Robert L.: Flow and Pressure Field Analysis of Parallel Groove Geometry for an Incompressible Fluid with Convective Inertia Effects. NASA TN D-3635, 1966.

17. Zotov, V. A.: Research On Helical Groove Seals. Russian Eng. J., vol. 10, Oct. 1959, pp. 3-7.

18. Stair, William K.: Analysis of the Viscoseal. Part I: The Concentric Laminar Case. NASA CR-285, 1965.

19. Smith, M. I.; and Fuller, D. D.: Journal-Bearing Operation at Superlaminar Speeds. Trans. ASME, vol. 78, no. 3, Apr. 1956, pp. 469-474.

20. Ng, Chung-Wah; and Pan, C. H. T.: A Linearized Turbulent Lubrication Theory. J. Basic Eng. vol. 87, no. 3, Sept. 1965, pp. 675-688.

21. Stair, William K.; and Hale, Robert H.: Analysis of the Viscoseal. Part II: The Concentric Turbulent Case. Rep. ME-66-587-7, Tennessee (NASA CR-76866), June 28, 1966.

22. Anon.: Fundamentals of Friction and Lubrication in Engineering; First ASLE National Symposium. 1954.

NASA-Langley, 1969 —— 15 E-4782